



Facile solution synthesis of tin sulfide nanobelts for lithium-ion batteries



Keyu Li ^a, Shancheng Yan ^{a,*}, Zixia Lin ^b, Yi Shi ^{c,**}

^a School of Geography and Biological Information, Nanjing University of Posts and Telecommunications, Nanjing 210023, PR China

^b National Laboratory of Solid State Microstructures, Nanjing University, Nanjing 210093, PR China

^c Collaborative Innovation Center of Advanced Microstructures, Nanjing University, Nanjing 210093, PR China

ARTICLE INFO

Article history:

Received 31 December 2015

Received in revised form

25 April 2016

Accepted 26 April 2016

Available online 27 April 2016

Keywords:

SnS nanobelts

Hydrothermal approach

Anode materials

Lithium-ion batteries

High reversible capacity

ABSTRACT

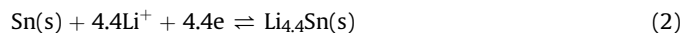
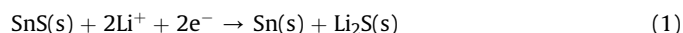
Two-dimensional Sn-based metal compounds (e.g. SnS, SnS₂ and SnO₂) are exceptionally attractive due to their excellent ion intercalation response and are suitable for use in energy storage devices (e.g. lithium-ion batteries and supercapacitors). However, the application of these dichalcogenides in Li-ion batteries is hindered by limitations in large-scale solution synthesis of SnS nanobelts. In this study, we developed a universal hydrothermal approach for the synthesis of SnS nanobelts and proposed an underlying mechanism for the formation reaction. When used as anode materials for lithium-ion batteries, SnS nanobelts maintain a discharge capacity of 889.9 mAhg⁻¹ after 50 cycles at a current density of 0.1 A/g. The nanobelts also exhibit high electrochemical performance, high rate capacity, and high reversible capacity. These results demonstrate that SnS nanobelts are potential anode materials for high-performance energy storage applications.

© 2016 Elsevier B.V. All rights reserved.

1. Introduction

Sn-based materials have gained considerable attention as future-generation Lithium-ion batteries (LIBs) due to their low cost, high theoretical capacity and large number of potential applications that hinges upon the electrical properties [1–9]. Amongst such materials, SnS possesses an orthorhombic structure, where tightly bound Sn–S atoms are connected by the van der Waals forces [10,11]. The crystallographic feature can facilitate Li⁺ diffusion, and functions as the buffering layer to compensate for large volume changes [12]. Moreover, SnS is low-cost, nontoxic, abundant and heavy metal-free [11]. With its high specific capacity, low cost, nontoxicity, and high electrical conductivity, SnS is a promising material for various applications, such as in LIBs, field-emission applications, photodetector devices, photocatalysts, and optoelectronics [11,13–21]. SnS with various nanostructures have been successfully synthesized through different methods [11–19,22–24]. Nevertheless, the following issues are still inevitable: 1) synthesis is complicated and mostly requires the use of hexamethyldisilazane and annealing treatment under high

temperature in N₂ gas; [5,12]; 2) limited control of SnS phase and morphology [11,14,18,23]; 3) and poor electrochemical properties due to excessive volume expansion during cycling [25]. The electrochemical reaction mechanism between SnS and lithium ions is generally proposed as follows [12,14,26,27]:



The first-step of the reaction has generally been considered to be irreversible and the theoretical capacity of SnS is calculated to be 782 mAhg⁻¹ (4.4Li/Sn) based only on the second step. It should be noted that the theoretical capacity of SnS based on the theoretical maximum (6.4Li/Sn) is 1138 mAhg⁻¹ if Li₂S can be decomposed completely according to the reversible reaction (SnS + 6.4Li⁺ + 6.4e⁻ ↔ Li_{4.4}Sn + Li₂S) [28–31]. Recent reports have also suggested that SnS₂ can realize a reversible conversion (formation and decomposition of Li₂S) via a probable novel mechanism for the storage of Li⁺ [29,30]. Therefore, it will be a significant challenge to explore a simple, environmentally friendly, controllable and rational synthesis design for SnS with high reversible capacity.

In this study, SnS nanobelts were synthesized via a simple,

* Corresponding author.

** Corresponding author.

E-mail address: yansc@njupt.edu.cn (S. Yan).

facile, and controllable hydrothermal route by controlling the change in solution color and state during the mixing stage, which allows the realization of controllable morphology for the final products. Contrary to previous reports, it has been found that the Tin source for the transformation of valence state for high reversible capacity is Sn^{4+} instead of Sn^{2+} . When applied to electrochemical tests as a potential anode for LIBs, SnS nanobelts maintained a discharge capacity of 889.9 mAhg^{-1} after 50 cycles at a current density of 0.1 A/g . SnS nanobelt anode also delivers a charge capacity of 890.3 mAhg^{-1} after 50 cycles reversibly and retrieves 5 Li^+ per Sn atom, corresponding to the reversibility of the conversion reaction ($\text{Sn} + \text{Li}_2\text{S} \rightarrow \text{SnS} + 2\text{Li}^+ + 2\text{e}^-$); as high as 30% of Li_2S can be decomposed according to the reversible reaction [28–30]. Hence, these materials exhibit good electronic connectivity, high charge/discharge capacity, and stable cycle performance.

2. Experimental details

2.1. Preparation of SnS nanobelts

In the typical experiment, 1 mmol $\text{SnCl}_4 \cdot 5\text{H}_2\text{O}$ and 2.5 mmol $\text{Na}_2\text{S} \cdot 9\text{H}_2\text{O}$ are dissolved in 30 ml of ethylene glycol by magnetic stirring to form a yellow solution. The mixture is placed into a 50 ml Teflon-lined autoclave that is maintained in an oven at 180°C for 24 h. After cooling to room temperature, the black precipitates are collected from the solution through centrifugal filtration, washed several times using distilled water to remove the organic residues, and dried at 60°C for 4 h. As a comparison, the same experiment is conducted using $\text{SnCl}_2 \cdot 2\text{H}_2\text{O}$ as a replacement for $\text{SnCl}_4 \cdot 5\text{H}_2\text{O}$.

2.2. Materials characterizations

Field emission scanning electron microscopy (FE-SEM; JSM-7000F) was used to determine the morphology of the samples. Transmission electron microscopy (TEM) and high-resolution transmission electron microscopy (HRTEM) images were obtained using a JEOL model JEM2100 instrument at an accelerating voltage of 200 kV. The crystal phase properties of the samples were analyzed with a Bruker D8 Advance X-ray diffractometer (XRD) using Ni-filtered $\text{Cu K}\alpha$ radiation at 40 kV and 40 mA at 2θ ranging from 10° to 90° with a scan rate of 0.02° per second. An FTIR spectrum was carried on NEXUS870 spectrometer from 2000 cm^{-1} – 200 cm^{-1} . Raman spectra were obtained on a Raman spectrometer (JY T64000) excited by the 514.5 nm line of an Ar⁺ laser under $100 \mu\text{W}$. X-ray photoelectron spectroscopy (XPS) analysis (PHI5000 Versaprobe) was used to determine the chemical composition of the products.

2.3. Electrochemical measurements

For lithium ion battery measurements, slurry of active material was prepared with carbon black and polyvinylidene fluoride (PVDF) in a weight ratio of 8:1:1, to form homogeneous slurry in N-methylpyrrolidone (NMP). This was then deposited as a film of thickness $50 \mu\text{m}$ on a copper foil and dried in vacuum at 80°C for 12 h. The electrodes were pressed to enhance the contact between the active materials and the conductive carbon. Coin cell assembly was done at room temperature in a glove box under argon. The mass loading of the active material on the working anode electrode was about 0.108 mg. Cyclic voltammograms and galvanostatic charge/discharge cycling were performed at current rates (0.1 A/g) in the voltage range of 0.1 and 1.2 V (versus Li^+/Li). The discharge capacity of SnS electrodes were performed at current density of 0.1, 0.2, 0.4 and 0.8 Ag^{-1} . The first five cyclic voltammograms (CV) over a

voltage range of 0.01–3.00 V at a scanning rate of 0.1 mV/s . Electrochemical impedance spectroscopy (EIS) of the fresh cell and after-cycling electrodes obtained by applying a sine wave with an amplitude of 5.0 mV over the frequency range of 1000 kHz – 0.01 Hz .

3. Results and discussion

To study the microsphere structure of samples prepared at 180°C for 24 h, we performed field-emission scanning electron microscopy (FESEM) analysis (Fig. 1a). The morphology of the prepared SnS comprises a large number of nanobelts with lengths of up to several microns. The nanobelt structures may allow the compensation of volume changes and improve cycling performance and stability during Li^+ insertion and deinsertion. The structural and morphological features were investigated by TEM (Fig. 1b). SnS nanobelts are about 150 nm wide. Parallel fringes appear in the HRTEM image (Fig. 1c) and are indicated by the red circle (Fig. 1b). These fringes have a typical spacing of 0.21 nm and are assigned to the (102) lattice planes of the orthorhombic SnS structure. Based on the selected area electron diffraction (SAED) patterns (Fig. 1d), SnS nanoribbons exhibit a single crystalline structure [16,19]. The three characteristic diffraction peaks of (011), (1-11) and (102) belonging to the same zone axis are shown in Fig. 1d, as denoted by white letter; this finding is consistent with the XRD patterns shown in Fig. 2d (red) [32].

X-ray photoelectron spectroscopy (XPS) analysis was performed to investigate the surface chemical composition of the prepared samples. The binding of specimen charging is corrected by referencing C 1s to 284.60 eV. As shown in Fig. 2a, no other peaks of elements other than Sn, S, O, and C were observed. The presence of two strong peaks at 494.85 and 486.35 eV corresponds to the two binding energies of $\text{Sn}^{2+}3\text{d}_{3/2}$ and $\text{Sn}^{2+}3\text{d}_{5/2}$, respectively, because of the spin-orbit interaction in the metal sulfide (Fig. 2b). The spacing between the two peaks is about 8.50 eV, which indicates the energy gap between $\text{Sn}3\text{d}_{5/2}$ and $\text{Sn}3\text{d}_{3/2}$. The S 2p spectrum shows S 2p at about 161.475 eV (Fig. 2c). This result is consistent with previous reports on SnS [13,14].

It is interesting that the color and state of the solution color change with the transformation of valence state ($\text{Sn}^{4+} \rightarrow \text{Sn}^{2+} \rightarrow \text{Sn}^{4+}$) when the Tin source is Sn^{4+} instead of Sn^{2+} during different solution mixed phases. To explore the evolution of the morphology, the study is conducted by controlling the solution with mixed color and state. The XRD patterns show that the structures of the sample differ at different stages (Fig. 2d). The diffraction of hexagonal SnS_2 corresponds to stages 1 (light yellow transparent liquid) and 3 (yellow turbid solution) (JCPDS 23-0667), and the standard diffraction of the orthorhombic SnS corresponds to stage 2 (yellow solution) (JCPDS 65-3812) [12,25,33]. The XRD pattern of the typical sample with stage 2 (yellow solution) is shown by the red line. Six strong characteristic diffraction peaks of (111), (400), (011), (201), (210), and (311) are indexed to the standard diffraction data of the orthorhombic SnS (JCPDS 65-3812) [12,13,32]. No peak is attributed to SnS_2 in the prepared samples, indicating the highly pure orthorhombic phase of SnS. The sharp and strong peaks also indicate that the as-synthesized SnS products are well-crystallized. These results reveal that the differences between morphology and product composition are affected by mixing stages with changes in color and state.

In the experiment, the solution mixing stage has vital influences on the phase change and the properties of the final product. As shown in Fig. 3a, changes in color and state are detected as light yellow transparent liquid, yellow solution and yellow turbid solution (first-line). Changes in color and state are evident in the solution. To explore the influence of the mixing stage on the

Download English Version:

<https://daneshyari.com/en/article/1605589>

Download Persian Version:

<https://daneshyari.com/article/1605589>

[Daneshyari.com](https://daneshyari.com)